Anisotropy of ion-beam-induced self-diffusion in pyrolytic graphite

B. Söder, J. Roth, and W. Möller
Max-Planck-Institut für Plasmaphysik–EURATOM Association, D-8046 Garching bei München, Federal Republic of Germany
(Received 30 June 1987)

The ion-beam-induced self-diffusion in pyrolytic graphite (HPG) has been investigated. In order to look for anisotropic effects two target orientations have been chosen, one with the basal planes perpendicular to the surface (HPG-edge) and a second one with the planes parallel to it (HPG-base). Samples preimplanted with a ^{13}C marker were bombarded with 20-keV D^+ ions at different temperatures. The ^{13}C depth profiles were analyzed by Rutherford backscattering (RBS) using 2.0- and 2.6-MeV $^4He^+$ ions. Strong effects of anisotropy are found for different target orientations despite the high damage levels. A simulation of the marker diffusion is presented which is based on radiation damage and the behavior of moving defects in graphite. The theoretical description is in good agreement with the experimental results if suitable rate constants of interstitial-vacancy recombination and vacancy-vacancy annihilation are chosen. The orientational effects are explained by an interstitial diffusion which proceeds mainly parallel to the graphite planes.

I. INTRODUCTION

Graphite with a variety of different structures is widely used in fission reactors and also in fusion experiments. In these applications the material is either bombarded with neutrons or with different ions at temperatures often exceeding 1000 K. There have been many investigations on the influence of radiation on a variety of physical properties. These include studies on the production and annealing of radiation damage,[1] the neutron swelling on the *c*-axis direction[2] and, as one of the latest results, the growing of pores under particle radiation.[3] These radiation effects are based on the additional mobility of carbon atoms due to bombardment. Kelly published a model of radiation damage in graphite[4] which is in good agreement with the macroscopic observations of *c*-axis swelling and *a*-axis contraction and their dependence on neutron fluence and temperature. There the diffusion in graphite is governed by the interstitials, while vacancies only become mobile above 1200 K. Until recently there has been no direct confirmation of this theory on the microscopic scale. Roth *et al.*[5] explained the radiation-enhanced sublimation of graphite on the basis of the radiation damage model as a consequence of migration of the interstitials. The decrease of the ion-beam-induced self-diffusion due to doping with impurities,[6] in this picture, would be a consequence of the trapping of interstitials at these impurities. Owing to the anisotropy of the graphite structure, migration of interstitials parallel to the planes would lead to anisotropic radiation-induced diffusion, which is also indicated by the observation of in-plane migration of impurities by Elman *et al.*[7]

Earlier investigations[8] were concerned with the ion-beam-induced self-diffusion of a ^{13}C- marker profile in pyrolytic graphite (HPG) cut parallel to the lattice planes. The proposed model of Roth *et al.* could explain the temperature dependence of the effective diffusion coefficient of carbon quite well. It did not, however, take the anisotropy of the graphite structure into account and, as a consequence, the changes of the ^{13}C profile shapes could not be reproduced. This work is concerned with the anisotropy of the radiation-enhanced diffusion. Therefore two kinds of targets, one with the target surface parallel to the basal planes (HPG-base) and the other with the surface perpendicular to the planes (HPG-edge) have been investigated. The preliminary model[8] was modified in order to describe the marker profile changes and their dependence on crystal orientation.

II. MODEL

Radiation damage in graphite has been investigated since the early 1940's, especially with respect to neutron irradiation in fission reactors. The most comprehensive radiation damage theory was developed by Kelly.[4] It is assumed that Frenkel pairs produced by radiation diffuse in the graphite lattice. The macroscopic contraction of the material parallel to the lattice planes is caused by the collapse of vacancy lines, while the *c*-axis swelling is a consequence of clustering of interstitial atoms to dislocation loops forming extra lattice planes. The loop formation occurs at preexisting nuclei and a density of nuclei ranging from 10^{16} to 10^{17} cm^{-3} could be deduced. The mobility of interstitials was assumed to be high already at room temperature, while vacancies get mobile only above 1200 K. The theory allowed for recombination of vacancies and interstitials. A recombination barrier of 0.28 eV was deduced from the temperature dependence of swelling.

The application of this theory to the case of near-surface ion irradiation has been treated earlier.[8] In the following, the underlying processes of our model are discussed. Again it is assumed that the incoming deuterium ions produce Frenkel pairs. The rate of Frenkel pair production $S_F(x)$ for a given ion flux can be calculated as the number of energy transfers per unit volume above

a certain displacement threshold E_d. For the present work $S_F(x)$ was taken from Monte Carlo binary collision simulations by means of the TRIM program[9] using $E_d=25$ eV.

At sufficiently high temperatures both interstitials and vacancies may diffuse through the graphite with diffusion coefficients

$$D_i=D_i^0\exp(-E_i/kT)\ ,$$

$$D_v=D_v^0\exp(-E_v/kT)\ . \tag{1}$$

A diffusion-controlled recombination rate with a recombination radius R_{iv} is assumed[10] for the recombination of interstitials and vacancies. As in Kelly's model, a recombination barrier with an additional activation energy E_{iv} and a preexponential factor R_{iv}^0 is introduced.[11] The collapse of vacancy lines cannot be treated adequately in the one-dimensional model. We therefore simulate it by diffusion-controlled annihilation of vacancies within an annihilation radius R_{vv}.

For the special case of ion implantation, the local concentration of vacancies, c_v, may become exceedingly high, especially at low temperatures, such that spontaneous recombination and annihilation of additionally generated interstitials and vacancies become significant.

Considering these spontaneous processes one has to estimate the corresponding probabilities of their occurrence: The probability for spontaneous recombination of a Frenkel pair produced close to a vacancy is $P_r=c_v(v_i+v_v)$, with v_i and v_v being the recombination volumes of interstitials and vacancies, respectively. Analogously the probability for spontaneous annihilation is $P_a=2c_vv_v$. In consequence, the source terms for the interstitials and vacancies are

$$S_{Fi}=S_F(1-P_r)=S_F[1-c_v(v_i+v_v)]\ , \tag{2}$$

$$S_{Fv}=S_F(1-P_r-2P_a)=S_F[1-c_v(v_i+v_v)-4c_vv_v]\ , \tag{3}$$

because two vacancies disappear in one annihilation process. According to Duesing *et al.*[12] we have to consider the overlap of the recombination volumes, which results in the effective recombination volumes v_i and v_v. It is only necessary for the vacancies, as the interstitial concentration c_i is small in the present temperature range:

$$v_i=v_0^i\ , \tag{4}$$

$$v_v=v_0^v-\tfrac{1}{2}c_vv_0^v\ , \tag{5}$$

where v_0^v and v_0^i denote the annihilation and recombination volumes, respectively, in the limit of small defect concentrations. Thus the source terms become

$$S_{Fi}=S_F[1-c_vv_0^i-c_vv_0^v(1-\tfrac{1}{2}c_vv_0^v)]\ , \tag{6}$$

$$S_{Fv}=S_F[1-c_vv_0^i-5c_vv_0^v(1-\tfrac{1}{2}c_vv_0^v)]\ . \tag{7}$$

Any clustering of interstitials is neglected in the presented model.

The experimental situation which has to be simulated by our calculation is the ion-beam-induced diffusion of the ^{13}C-marker profile in the ^{12}C-graphite matrix. In consequence, the mathematical treatment has to consider all the processes discussed before, both for ^{12}C and for ^{13}C.

The mathematical description is done by a set of coupled rate equations, the solutions of which are the concentrations of atoms occupying a lattice site, c^{12} and c^{13}, interstitial atoms, c_i^{12} and c_i^{13}, and vacancies c_v as functions of time t and depth x.

$$\frac{\delta c^{12}}{\delta t}=4\pi\rho R_{iv}^0\exp(-E_{iv}/kT)D_ic_vc_i^{12}-S_{Fi}c^{12}\ , \tag{8}$$

$$\frac{\delta c^{13}}{\delta t}=4\pi\rho R_{iv}^0\exp(-E_{iv}/kT)D_ic_vc_i^{13}-S_{Fi}c^{13}\ , \tag{9}$$

$$\frac{\delta c_i^{12}}{\delta t}=D_i\frac{\delta^2c_i^{12}}{\delta x^2}-4\pi\rho R_{iv}^0\exp(-E_{iv}/kT)D_ic_vc_i^{12}+S_{Fi}c^{12}\ , \tag{10}$$

$$\frac{\delta c_i^{13}}{\delta t}=D_i\frac{\delta^2c_i^{13}}{\delta x^2}-4\pi\rho R_{iv}^0\exp(-E_{iv}/kT)D_ic_vc_i^{13}+S_{Fi}c^{13}\ , \tag{11}$$

$$\frac{\delta c_v}{\delta t}=D_v\frac{\delta^2c_v}{\delta x^2}-4\pi\rho R_{iv}^0\exp(-E_{iv}/kT)D_ic_v(c_i^{12}+c_i^{13})-8\pi\rho D_vR_{vv}c_v^2+S_{Fv}(c^{12}+c^{13})\ . \tag{12}$$

The indices "12" and "13" denote the different carbon isotopes. All concentrations are given in atomic units, i.e., relative to the number of host atoms per unit volume, ρ.

The initial condition is given by the ^{13}C implantation profile, no interstitials exist at this time, while the boundary condition is controlled by the flux of carbon atoms leaving the surface, given by

$$j^{12,13}=K_0\exp(-E_{\mathrm{Des}}/kT)c_i^{12,13}(x=0)\ . \tag{13}$$

K_0 is the rate constant for the sublimation of carbon atoms from the surface. In this model the flux of carbon atoms leaving the surface is thermally activated with the activation energy E_{des}. The ratio between the integral of desorbing carbon atoms and the number of incoming D^+ ions is equivalent to the sputtering yield Y.

The solution of the system is calculated by a special version of the one-dimensional PIDAT diffusion program.[13] A disadvantage of the calculations is the appearance of physically unrealistic local excess or depletion of the density of the graphite due to the neglected contraction or swelling. For example, an interstitial diffusing out of the depth interval Δx will decrease the number of atoms in this volume, which is the local density. The influence of this effect is discussed later.

Graphite crystals have a high anisotropy because of the planar structure [Fig. 1(a)]. The binding energy of the carbon atoms is very high inside the plane (5 eV), but less between the planes (0.17 eV). The intraplane atomic distance is 1.4 Å and the interplane atomic distance 3.5 Å. While the diffusion coefficient for interstitials and vacancies parallel to the planes are well known, the corresponding values perpendicular to the planes are much smaller and subject to a large uncertainty,[14] and are neglected in the further treatment. If diffusion coefficients for interstitials and vacancies are taken from literature, the described model is applicable to the case of graphite with planes oriented perpendicular to the surface (HPG-edge).

However, the same model has also been applied to HPG-base. These samples are characterized by their surface being parallel to the basal planes, but because of a mosaic spread of 18.8° this property is not strictly valid for the graphite used in our experiment. Therefore one can define an average absolute tilt angle α of the planes with respect to the surface. It is still assumed that the interstitials are migrating parallel to the planes, i.e., parallel to $x'=x/\sin\alpha$ [Fig. 1(b)]. Migration perpendicular to the planes is neglected. Because of the average misalignment α of the planes they have a migration component in the x axis. The diffusion equations are the same as for HPG-edge but one has to consider the transformation $x=x'\sin\alpha$ from the x' system to the x system in Eqs. (8)–(12) and also in the boundary and initial conditions. For example, Eq. (8) is replaced by

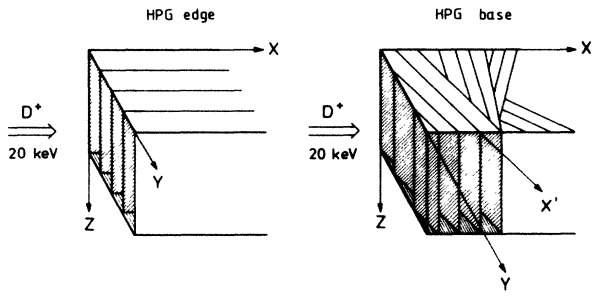

FIG. 1. Structural anisotropy of graphite. The left part of the figure (a) symbolizes the orientation called HPG-edge, where the basal planes are perpendicular to the surface, which is located at $x=0$. The right part (b) shows the sample called HPG-base with a mean orientation of the basal planes parallel to the surface. The mosaic spread is indicated by the misalignment of some crystallites, where α is the angle between Y and x'.

$$\frac{\delta c^{12}(x')}{\delta t}=4\pi\rho R_{iv}^{0}\exp(-E_{iv}/kT)\times D_i c_i^{12}(x')c_v(x')-S_{Fi}(x')c^{12}(x') \quad (14)$$

In this respect the present treatment differs from earlier work for HPG-base,[8] where lattice anisotropy was not considered.

III. EXPERIMENTAL

The experimental procedure is similar to that used in an earlier investigation.[8] The samples are made of high purity graphite (HPG) with a size of 40×5 mm^2, a thickness of 0.2 mm and a density of 2.24 g/cm^3. These strips were mechanically polished. Their mosaic spread, measured with Cr $K\alpha$ radiation, was 18.8°. As indicated in Fig. 1, two different orientations of this graphite were examined, one called HPG-edge with the surface perpendicular to the basal planes, and the other called HPG-base with the surface parallel to the planes.

We have chosen ^{13}C as a marker for the self-diffusion. Chemically, ^{13}C should react like ^{12}C. According to classical diffusion theory the difference in mass between the isotopes results in a slightly different jump frequency.[15] In our case of ^{13}C and ^{12}C the error is less than 4%.

The graphites were implanted with 10 keV ^{13}C perpendicular to the surface with magnetically analyzed ion beams using 99% enriched ^{13}CO as source gas.[16] The implantation spot was bigger than the target size, resulting in a uniform lateral distribution with negligible concentration gradients parallel to the surface. The ^{13}C-concentration profiles have a maximum of about 25 at % ^{13}C at a depth of 40 nm. After transfer to the analysis chamber, ion bombardment and Rutherford backscattering (RBS) analysis were performed *in situ* at different temperatures. Before ion mixing was performed the samples were tempered to 1423 K for 10 min. After this treatment no change in the initial ^{13}C-depth profiles could be detected for both HPG-base and HPG-edge. 20 keV D^+-ions at a flux of 8×10^{15} D^+/cm^{2}s caused ion beam mixing. A sweep produces a homogeneous D^+-implantation area with a diameter of 2 mm. Figure 2 shows the depth distribution of produced Frenkel pairs calculated with the TRIM program,[9] which is equivalent to the source term $S_F(x)$ of the rate equations. The mean depth of the Frenkel pair production by deuterons at this energy is about ten times the range of the ^{13}C in graphite. It can be seen that the production rate of interstitials and vacancies in the first 100 nm, where the ^{13}C is situated, is nearly constant with depth. One can calculate from Fig. 2 that at a depth of 50 nm and at a fluence of 8×10^{18} D^+/cm^2 about 16 displacements per atom (dpa) are obtained.

RBS depth profiling of the ^{13}C marker was executed *in situ* with $^4He^+$ ions with energies of 2.0 and 2.6 MeV. For conversion into depth profiles in this energy range an enhancement of the $^{13}C(\alpha,\alpha)$ ^{13}C scattering cross section has to be taken into account.[17] The LORI program[18] was used to transform the spectra to depth profiles. For

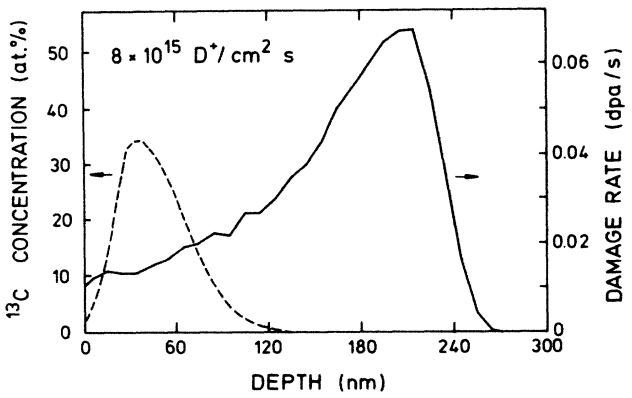

FIG. 2. The source term $S_F(x)$ has been calculated with the Monte Carlo simulation TRIM for a D^+ flux of 8×10^{15} $D^+\,cm^{-2}s^{-1}$. S_F gives the displacements per atom and time as function of depth. In the first 100 nm the depth dependence of S_F is very small. The initial ^{13}C distribution is also indicated.

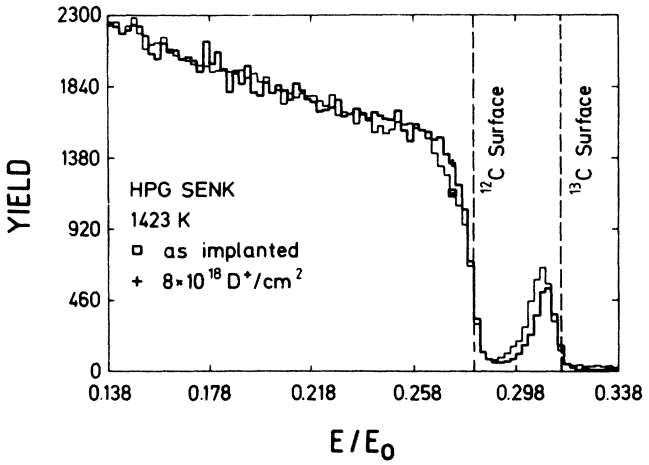

FIG. 3. Here we show two experimental RBS spectra. The analyzing ions were $^4He^+$ at 2.6 MeV. The spectrum indicated with (——) is that of HPG-edge before D^+ mixing. The peak of ^{13}C is resolved from the ^{12}C-bulk signal. The energies of α particles backscattered from ^{12}C and ^{13}C at the surface are marked. The second spectrum (+) has been taken from the same sample after mixing with 8×10^{18} D^+/cm^2 at 1423 K. A decrease of the ^{13}C peak is clearly revealed, while the ^{12}C-bulk signal has not changed.

the interpretation of the derived profiles the depth resolution of the method of analysis has to be taken into account. Theoretical calculations of the depth resolution[19] yield values between 28 nm at the surface and 33 nm at a depth of 150 nm.

The temperature during ion beam mixing was varied from room temperature to 1423 K by resistance heating. Temperatures exceeding 1100 K were measured by pyrometry. Ion beam mixing at room temperature resulted in implantation and trapping of hydrogen accompanied by additional energy loss of the backscattered helium. At temperatures of 1173 K and above, no trapped hydrogen could be detected by RBS after ion beam mixing. Some of the sample surfaces were monitored by scanning electron microscopy[20] (SEM) and, as reported in Ref. 21, small cracks could be observed in the case of HPG-base samples.

IV. RESULTS AND DISCUSSION

Figure 3 shows two Rutherford Backscattering spectra of HPG-edge before and after ion beam mixing at 1423 K. One can see that the ^{13}C signal is well resolved from the ^{12}C bulk signal. Except for the surface layers the backscattering signal from the ^{12}C bulk has not changed. But one can recognize the shrinkage of the ^{13}C profile, while the broadening is very small. The position of the surface of the ^{12}C and ^{13}C signals is indicated. The mass resolution of ^{12}C and ^{13}C increases with the energy of the analyzing $^4He^+$ ions, 2.6 MeV have been chosen in this case. These spectra are transformed to ^{13}C depth profiles which can be seen in Figs. 4(a) and 5(a) respectively for HPG-base. The temperature and the fluence of the implanted D^+ ions are chosen as parameters in these figures. For both kinds of targets three temperatures and fluences up to 8×10^{18} D^+/cm^2 are shown. To exclude thermal diffusion and mixing by the analyzing $^4He^+$ ions,[22] the samples were heated to 1423 K for 10 min before mixing. The depth profiles showed no significant differences before and after the heat treatment.

A difference in the behavior between HPG-base and HPG-edge is evident. In order to quantify the difference a spectrum is fitted by three components: an asymmetric Gaussian for the ^{13}C peak, an error function for the ^{12}C-edge, and a linear background function. The depth profiles of Fig. 4(a) and 5(a) are those obtained after this procedure. Then the moments of zeroth to third order of the profiles were calculated, these being the integral I, the mean depth M, the variance σ^2 and the skewness S. These moments were plotted versus the D^+ fluence. We just select the integral and the variance for discussion, the first in order to draw attention to the loss of ^{13}C and the latter because in mixing experiments the ratio $\Delta\sigma^2/\Delta\Phi$, with the variance σ^2 and the fluence of mixing ions Φ, is a characteristic value for the effective diffusivity in ion-induced mixing experiments.[23] Figure 6(a) compares the experimental values of the ^{13}C integral indicated by points (HPG-base) and crosses (HPG-edge) with those obtained by the calculations (lines). One can see that the integral of the ^{13}C profile of HPG-edge decreases very quickly with the fluence of 293 K, while the integral of the ^{13}C profile of HPG-base rests nearly constant. This behavior can be even seen directly in the corresponding depth profiles of Figs. 4(a) and 5(a). It cannot be concluded that the missing ^{13}C in HPG-edge has all left the graphite. One has to bear in mind that the profiles are obtained from the RBS spectra (Fig. 3). From the decrease of the integrals one can just make the statement that the ^{13}C has left the first 100 nm. α particles backscattered by ^{13}C at larger depths cannot be resolved from α particles backscattered by ^{12}C.

Also, the variance reveals a difference in the two

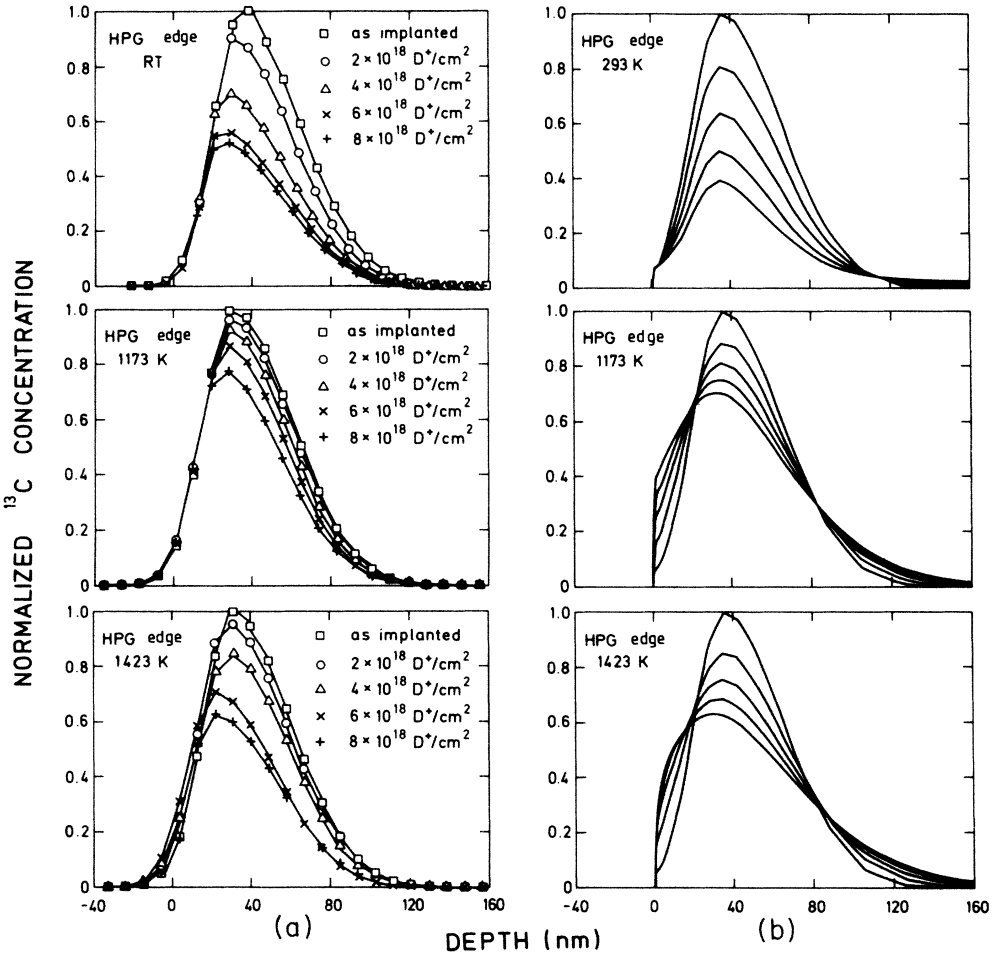

FIG. 4. The left part of the figure (a) shows the experimental depth profiles of the ^{13}C marker in HPG-edge. A set of profiles is given for three different temperatures: 293, 1173, and 1423 K. Each set of profiles consists of five profiles of the marker for different D^+ fluences. The right part (b) shows the corresponding profiles of the calculation for the same temperatures and D^+ fluences of 0, 2×10^{18}, 4×10^{18} 6×10^{18}, and 8×10^{18} D^+/cm^2.

orientations. Figure 6(b) shows the dependence of this moment on the D^+ fluence again in comparison with the calculated values. While the variance of the ^{13}C profile of HPG-base increases with the fluence as is observed in most mixing experiments, the profile in HPG-edge shows no broadening. This is a striking difference. The moments calculated with the presented model reveal a transient behavior with the ion fluence. These deviations from a linear relationship cannot be resolved in the experimental observations. In order to condense the experimental results a mean slope was fitted to the experimental values in Fig. 6. In Table I these mean slopes $\Delta I/\Delta\Phi$ and $\Delta\sigma^2/\Delta\Phi$ and additionally $\Delta M/\Delta\Phi$ and $\Delta S/\Delta\Phi$ are given at various temperatures. The table presents in a concentrated form the experimentally resolved differences in the behavior of the ^{13}C-marker in HPG-base and in HPG-edge. In HPG-edge samples the center of the ^{13}C profile is shifted to the surface whereas the center of the ^{13}C profile in HPG-base increases with the D^+ fluence. This behavior is maintained even at higher temperatures. The dependence of the skewness on the other hand varies with temperature and orientation. While the skewness of the ^{13}C profiles in HPG-base remains constant during ion-beam-induced diffusion, in HPG-edge the profiles become more asymmetric under bombardment, especially at room temperature. At higher temperatures this deviation disappears.

The aim of our model calculation is to simulate the profiles of different temperatures and D^+ fluences with one consistent set of parameters. In a first step we have applied the model to simulate the ^{13}C depth profiles in HPG-edge. The suitable parameter set can be seen in Table II. In Fig. 4(b) the calculated ^{13}C depth profiles in HPG-edge are shown for D^+ fluences of 0, 2×10^{18}, 4×10^{18}, 6×10^{18}, and 8×10^{18} D^+/cm^2 and for the three different temperatures. The strong decrease and the lack of broadening of the profiles with fluence at room temperature are well simulated. Both experiment and calculations show a peak shift towards the surface. The calculations reveal a ^{13}C tail at larger depths which cannot be seen in the experimental profile. But, as discussed above, this is not astonishing because any ^{13}C tail will be hidden in the ^{12}C bulk signal (Fig. 3). In order to control the reliability of the RBS profiles the ^{13}C profiles of

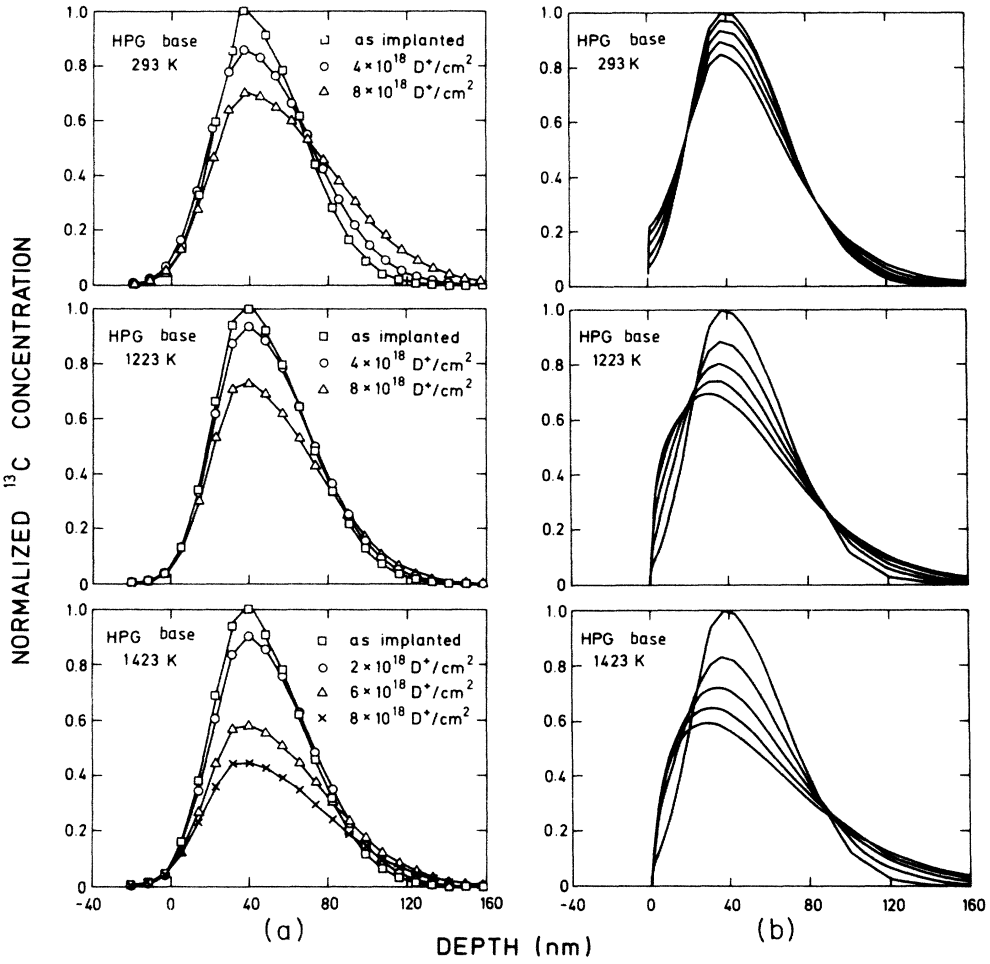

FIG. 5. The left part of the figure (a) shows the experimental depth profiles of the ^{13}C marker in HPG-base. A set of profiles is given for three different temperatures: 293, 1223, and 1423 K. Each set of profiles consists of several profiles of the marker for different D^+ fluences. The right part (b) shows the corresponding profiles of the calculation for the same temperatures and D^+ fluences of 0, 2×10^{18} 4×10^{18}, 6×10^{18}, and 8×10^{18} D^+/cm^2.

five samples were also measured by secondary ion mass spectroscopy (SIMS). The resulting profiles agree very well with these obtained by RBS except for HPG-edge at room temperature. Here, in addition to the profile measured by RBS, a ^{13}C tail at larger depths comparable to that of the calculated profile could be detected, as shown in Fig. 7.

Also the depth profiles calculated for higher implantation temperatures are in reasonable agreement with the experimental findings. It should be noted that the limited depth resolution of the analysis (see Sec. III) smears out steep slopes of the profiles. For example, the near-surface variation of the high-temperature profiles cannot be observed in detail experimentally.

The radiation-induced diffusion consists of the creation of a Frenkel pair and the diffusion of the interstitial between the planes until it recombines with a vacancy. Owing to the repulsive barrier between the interstitial and vacancy, the recombination rate is very low at room temperature and thus the interstitials will migrate a long distance until they are inserted in the graphite lattice. At 1173 K this recombination barrier is overcome; thus the migration distance is smaller and the recombination limits the broadening. This is accompanied by a smaller decrease of the profile integral within the analysed depth. At 1423 K the mobility of the vacancies becomes important, which results in vacancy depletion and in a greater broadening of the profiles than at 1173 K. At all temperatures the agreement between the experimental and calculated profiles is very good, with the exception that the profiles calculated for high fluences are systematically broader than the measured ones. This point will be treated in more detail below.

The parameters used in the calculation are summarized in Table II. The value of E_v is taken from literature;[14] with the atomic density ρ, D_i^0 and D_v^0 are assumed to be

$$D_i^0=D_v^0=\tfrac{1}{6}\times10^{13}\rho^{-2/3}\ \text{sec}^{-1}\ , \tag{15}$$

according to random walk theory in a three dimensional isotropic medium.[24] For HPG-edge the choice of $E_i=0.39$ eV is not critical. A similar fit can also be obtained with, for example, $E_i=0.1$ eV. The activation en-

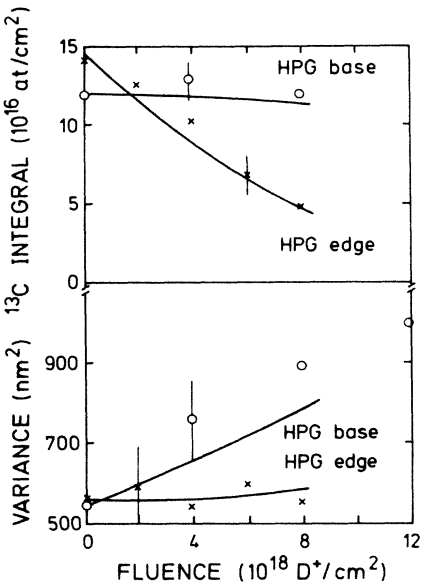

FIG. 6. The upper part of this figure (a) shows the integral of the ^{13}C profile as function of the D^+ fluence for both target orientations. While for HPG-base the integral is independent of the D^+ fluence, in HPG-edge it decreases with the fluence. (b) shows the dependence of the variance with the fluence for both targets again at room temperature. The ^{13}C profiles in HPG-edge reveal a lack of broadening. The lines indicate the corresponding values obtained by model calculations.

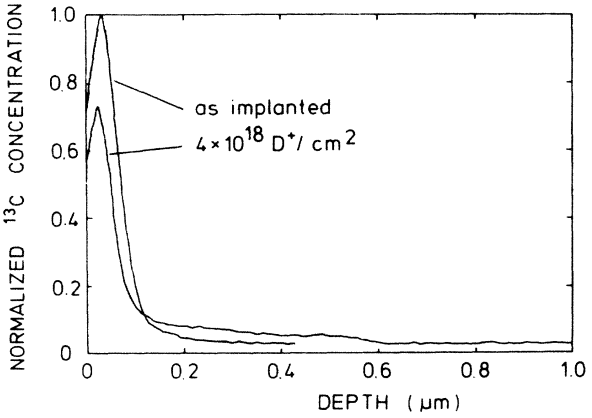

FIG. 7. The ^{13}C depth profiles presented here are obtained by SIMS measurements of HPG-edge before and after ion beam mixing with a fluence of 4×10^{18} D^+/cm^2 at room temperature. While the behavior of the marker localized up to a depth of 100 nm is in accordance with RBS analysis [Fig. 4(a)], after mixing an additional ^{13}C-tail is revealed in the bulk. The natural content of about 1 at.% ^{13}C produces the constant background.

ergy for in-plane migration of interstitials is 0.1 eV.[14] However, interstitials may also migrate as di-interstitials or larger clusters with different activation energies, which depend on their size and, in consequence, on the thermal stability.[25] The assumption of activated recombination is necessary to explain the large ranges of mobile defects at room temperature. It was necessary to choose a value of $E_{iv}=0.5$ eV somewhat higher than the

TABLE I. Experimentally resolved difference for the ^{13}C marker in HPG-base and in HPG-edge.

	Temperature (K)	HPG-edge (c perpendicular to surface normal)	HPG-base (c parallel to surface normal)
$\frac{\Delta\text{integral}}{\Delta(D^+\text{ fluence})}$ $\left[\frac{\text{atoms cm}^2}{\text{cm}^2\text{ ions}}\right]$	293	-0.016	0
	1173[a]	-0.004	-0.006
	1423	-0.008	-0.014
$\frac{\Delta\text{ center}}{\Delta(D^+\text{ fluence})}$ $\left[\frac{\text{cm}^3}{\text{ions}}\right]$	293	-5×10^{-26}	$+8\times10^{-26}$
	1173[a]	-5×10^{-26}	$+6\times10^{-26}$
	1423	-8×10^{-26}	$+10\times10^{-26}$
$\frac{\Delta\text{variance}}{\Delta(D^+\text{ fluence})}$ $\left[\frac{\text{cm}^4}{\text{ions}}\right]$	293	0	$+5\times10^{-31}$
	1173[a]	0	$+4\times10^{-31}$
	1423	$+1\times10^{-31}$	$+6\times10^{-31}$
$\frac{\Delta\text{skewness}}{\Delta(D^+\text{ fluence})}$ $\left[\frac{\text{cm}^2}{\text{ions}}\right]$ (skewness according to Charlier)	293	$+2.8\times10^{-24}$	0
	1173[a]	$+1.1\times10^{-24}$	0
	1423	0	0

[a]For HPG-base the temperature is 1223 K.

values of 0.24–0.30 eV (Ref. 26) obtained from neutron irradiation experiments. Considering that in our experiment the radiation damage was produced by deuterium it seems reasonable that the hydrogen may decorate the vacancies, especially at room temperature, which might increase the recombination barrier. For $R_{iv}^0 = 2.8 \times 10^{-6}$ cm and $R_{vv} = 2.9 \times 10^{-7}$ cm there are, to our knowledge, no literature data available, and they remain as free fit parameters. It is difficult to explain the values physically because they only determine the rate coefficient in connection with the diffusion coefficient and this relation depends on the model of diffusion-limited recombination and annihilation.

v_0^i is chosen to limit the maximum vacancy concentration to 1% by analogy to metals.[12] The choice of $v_0^v = 1$ implies that the spontaneous vacancy annihilation is limited to vacancies occupying adjacent lattice sites. Variations of v_0^v by a factor of 10 do not influence the results strongly. Its introduction, however, is necessary to yield an asymmetric creation rate of interstitials and vacancies by spontaneous annihilation of vacancies.

In order to test the error introduced by the occurrence of local density changes in the calculation, in one case we attempted to rearrange the depth scale of the resulting profiles to obtain a uniform density. Figure 8 shows these calculated profiles for HPG-edge at room temperature. A comparison with the equivalent experimental profiles in Fig. 4(a) shows even better agreement. This indicates that a dynamic program continuously rearranging the density might improve the description of the profiles. However, it should be recalled that the swelling and shrinkage by agglomeration of interstitials and annihilation of vacancies, respectively, which is macroscopically observed,[4] is not accounted for in the calculations up to now.

The model for HPG-edge has further been applied to

TABLE II. Summary of parameters used in the calculation.

Parameter name	Physical meaning	Value	Origin	Ref.
D_i^0	Preexponential factor of interstitial diffusion coefficient	7.3×10^{-2} cm^2/s	$D_i^0 = \frac{1}{6} \times 10^{13}\ \rho^{-2/3}$	24
D_v^0	Preexponential factor of vacancy diffusion coefficient	7.3×10^{-2} cm^2/s	$D_v^0 = \frac{1}{6} \times 10^{13}\ \rho^{-2/3}$	24
E_i	Activation energy of interstitial diffusion	0.39 eV		14
E_v	Activation energy of vacancy diffusion	3.1 eV		14
ρ	Atomic density of graphite	1.1×10^{23} atoms/cm^3		
E_{iv}	Activation energy of diffusion-dependent recombination	0.5 eV		4,26
R_{iv}^0	Preexponential factor of diffusion-dependent recombination	2.8×10^{-6} cm	Fit parameter	
R_{vv}	Rate factor of diffusion dependent annihilation	2.9×10^{-7} cm	Fit parameter	
v_0^i	Recombination volume of spontaneous recombination	100	Limits c_v to 1%	12
v_0^v	Annihilation volume of spontaneous annihilation	1	Assymetric source term for interstitials and vacancies	
S_F	Source term		TRIM Monte Carlo code	9
K_0	Preexponential factor of desorption	4.4×10^5 s^{-1}	Adjusted to 27	
E_{des}	Activation energy of desorption	0.8 eV	Adjusted to 27	

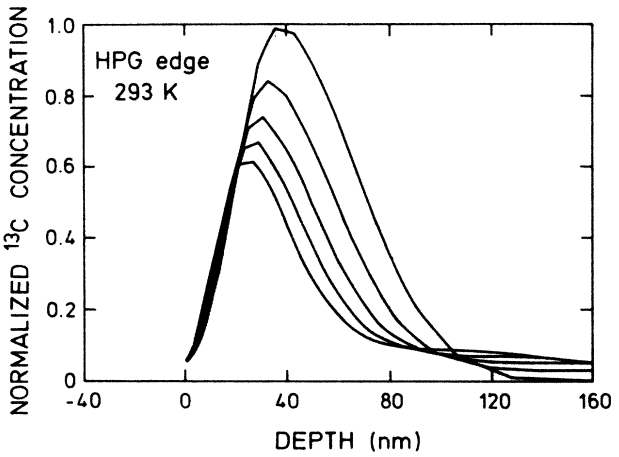

FIG. 8. Presented are calculated ^{13}C depth profiles in HPG-edge for fluences of 0, 2×10^{18}, 4×10^{18}, 6×10^{18}, and 8×10^{18} D^+/cm^2 at room temperature. The depth scale of the calculated profiles was rearranged to obtain a uniform density.

HPG-base. A realistic treatment would require the consideration of the whole angular distribution of the lattice planes given by the mosaic spread. But for the sake of simplicity the calculation was made for one crystallite, the c-axis of which was arbitrarily tilted by $\alpha=5.7°$ ($\sin\alpha=0.1$) to the normal of the target surface. The calculations were done with a set of transformed equations as indicated in Eq. (14) and suitable boundary and initial conditions. The main difference between HPG-base and HPG-edge lies in the fact that in the case of HPG-base the interstitial has to migrate a longer distance in the x' direction in order to cover the corresponding distance in the x direction. The results can be seen in Fig. 5(b) for the three different temperatures and D^+ fluences of 0, 2×10^{18}, 4×10^{18}, 6×10^{18}, and 8×10^{18} D^+/cm^2. At room temperature the experimental profiles can be simulated with the same set of parameters as for HPG-edge. Because of the smaller concentration gradient of ^{13}C parallel to x', the migration of interstitials is slower. In consequence the decrease of the ^{13}C profiles is less than in the HPG-edge sample at the same fluences. The recombination between interstitials and vacancies is very low at room temperature. However, at high temperatures it governs the processes. Here, good agreement between experiment and calculation could only be achieved in the present model by choosing a value of $*R_{iv}^0=3.4\times10^{-10}$ cm. We do not believe that the change of the fit parameter R_{iv}^0 can be physically interpreted in a direct way. Instead, it seems more realistic that it acts as a remedy for the insufficiency of our model.

One neglected process in our calculation is the contraction of the planes due to the collapse of vacancy lines and the corresponding swelling perpendicular to the planes due to interstitial clustering. This will lead to a contraction of the depth scale in the calculated HPG-edge profiles, while in the HPG-base profiles the contraction takes place perpendicularly to the direction of observation. Furthermore the smaller concentration gradient along x' in HPG-base makes the defect concentrations higher than in HPG-edge. So any cluster build up will be more effective in HPG-base than in HPG-edge. This might also lead to the migrating species being interstitials in one case and clusters in the other, with the consequence of different diffusion constants and different recombination probabilities. It also cannot be ruled out that at higher temperatures diffusion perpendicular to the planes takes place. However, this is known in thermal diffusion only at temperatures higher than 2500 °C. Finally, and probably most important, diffusing atoms can be transported across the planes by the sequence of Frenkel pair generation and a subsequent recombination at an adjacent lattice plane. This can be especially important when the free path length of the parallel diffusion is not much larger than the lattice spacing which is the case in the intermediate temperature range. From the rate constants of diffusion-controlled recombination given above, a mean-free-path length of about 5 nm at 1173 K is calculated, so that additional broadening could actually be expected for the HPG-base case.

Another value which can be calculated in our model is the flux of interstitial atoms reaching the surface. If it is assumed as in an earlier publication[5] that all interstitial atoms are desorbed, sputtering yields in accordance with experimental data[27] can be obtained at temperatures above 1000 K. At room temperature, however, convergence with the experimental results could only be achieved, assuming an activation energy of desorption of $E_{des}=0.8$ eV. This value is not in contradiction to the 0.15 eV of Philipps *et al.*[28] which has to be interpreted as the difference of the surface diffusion activation energy and the binding energy to the surface. Since, to our knowledge, experimental values of the sputtering yield for 20 keV D^+ on carbon do not exist in the full temperature range, we have applied our model to 1-keV D bombardment where an experimental data set is available. Figure 9 compares the experimental values and

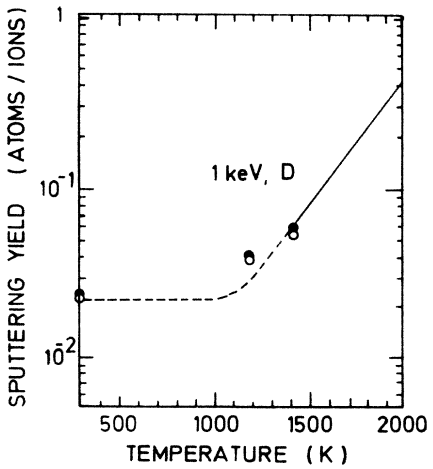

FIG. 9. Temperature dependence of the sputtering yield for 1-keV D^+ ions. The line interpolates the experimental values of Roth (Ref. 26), while the open points are the calculated sputtering yield for HPG-edge, as well as for 1-keV D^+ ions, and the solid points are those of HPG-base.

those calculated with the present model. The experimental values are interpolated by the line and the open points indicate the calculated result for HPG-edge, whereas the full points show those for HPG-base. The physical sputtering yield of $Y=2\times10^{-2}$ atoms/ion was added to the theoretical values. The temperature dependence of the sputtering yield is well reproduced. Another result of the calculation is that the sputtering yield of HPG-base exceeds that of HPG-edge, which is in excellent agreement with experiments by Hechtl *et al.* using oxygen[29] and different noble gases[30] as sputtering particles at different energies.

The difference between the preliminary calculations[8] and the model presented in this work is the additional consideration of the repulsive barrier for diffusion-dependent recombination and the activation energy of the desorption of carbon atoms from the surface. It seems that, despite the neglect of these two processes, the effective diffusion coefficient was reproduced quite well, but the simulation of the ^{13}C profiles was not satisfactory. This problem has been overcome now, and the behavior of a marker profile in graphite under the conditions of ion-beam-induced diffusion can be simulated with one consistent set of parameters. There remains a small discrepancy in the simulation of graphite, the planes of which are oriented parallel to the surface.

As a main result of the present work, it is surprising that the ion-induced self-diffusion of graphite still reveals prominent effects of orientation although the samples have been exposed to very high fluences of hydrogen bombardment, and thereby high levels of radiation damage. (The maximum fluence of 8×10^{18} D^+/cm^2 produces a damage of 16 dpa at a depth corresponding to the mean depth—see Fig. 2). However, this effect has also been observed in reflection high-energy electron diffraction (RHEED) studies by Gotoh.[31] It might be explained by the assumption that interstitials either recombine within the original planes or insert new planes by clustering, thus conserving the original direction of the planes.

V. CONCLUSION

The results of our investigation can be summarized as follows.

(i) The comparison of two differently oriented graphite samples, one with the *c* axis perpendicular to the surface and the other one with the *c* axis parallel to the surface, reveals a difference in the mixing of a ^{13}C marker under D^+ bombardment. This anisotropic behavior occurs in spite of the mosaic spread of the high-purity graphite and the considerable radiation damage and is in contrast to the isotropic thermal self-diffusion of carbon at temperatures above 2500 K.

(ii) The description of an effective self-diffusion coefficient in graphite from marker profile broadening alone leads to a loss of important information. The variation of the profile shape under particle bombardment has to be fully taken into account.

(iii) With the theory of radiation damage in graphite (Ref. 11) as a basis we developed a model for the radiation-induced diffusion in graphite. The calculated ^{13}C profiles agree well with those experimentally observed. For most parameters literature values could be found, the main free fitting parameters being the recombination volumes for interstitials and vacancies.

(iv) According to the model, the D^+-bombardment produces Frenkel pairs migrating thermally with activation energies of $E_v=3.1$ eV and $E_i=0.39$ eV in HPG-edge (*c*-axis parallel to the surface). For recombination a repulsive barrier with an activation energy of $E_{iv}=0.5$ eV must be overcome. Athermal recombination limits the vacancy concentration to 1%. According to the model D^+ mixing at room temperature leads to a ^{13}C tail deep in the sample. SIMS measurements provided experimental proof of this.

(v) In HPG-base (*c* axis perpendicular to the surface) we also assume inplane migration with a component perpendicular to the surface because of the mosaic spread of the graphite.

(vi) The calculated temperature dependence of the sputtering yield was in good agreement with experimental results. A surface barrier for desorption of 0.8 eV was chosen. The tendency of the sputtering yield to be higher for HPG-base than for HPG-edge, as published by Hechtl *et al.*,[30,31] was simulated very well by the model.

ACKNOWLEDGEMENT

The authors are indebted to E. Hechtl for the implantations of the ^{13}C markers and to K. Wittmaack for his skillful SIMS measurements of the marker profiles.

[1]T. Venkatesan, B. S. Elman, G. Braunstein, M. S. Dresselhaus, and G. Dresselhaus, J. Appl. Phys. **56**, 3232 (1984).
[2]B. T. Kelly and J. E. Brocklehurst Carbon, **9**, 783 (1971).
[3]E. Hoinkis, W. P. Eatherly, P. Krautwasser, and E. Robens, J. Nucl. Mater. **141/143**, 87 (1986).
[4]B. T. Kelly, Carbon **15**, 117 (1977).
[5]J. Roth and W. Möller, Nucl. Instrum. Methods B **7/8**, 788 (1985).
[6]B. Söder, J. Roth, and W. Möller, Nucl. Instrum. Methods B **19/20**, 832 (1987).
[7]B. S. Elman, G. Braunstein, M. S. Dresselhaus, and T. Venkatesan, Nucl. Instrum. Methods B **7/8**, 493 (1985).
[8]J. Roth, W. Möller, D. B. Poker, and K. Wittmaack, Nucl. Instrum. Methods B **13**, 403 (1986).
[9]W. Möller and W. Eckstein, Nucl. Instrum. Methods **132**, 814 (1984); Nucl. Instrum. Methods B **7/8**, 645 (1985).
[10]R. Sizmann, J. Nucl. Mater. **69/70**, 386 (1978).
[11]B. T. Kelly, *Physics of Graphite* (Applied Science, London, 1981).
[12]G. Duesing, W. Sassin, W. Schilling, and H. Hemmerich, Cryst. Lattice Defects **1**, 55 (1969).
[13]W. Möller, Max-Planck-Institut für Plasmaphysik, Report

No. 9/44, 1985 (unpublished).
[14]P. A. Thrower and R. M. Mayer, Phys. Status Solidi A **47**, 11 (1986).
[15]J. Philibert, *Diffusion et Transport de Matiere Dans les Solides*, (Monographies de Physique, Les Ulis, 1985).
[16]E. Hechtl, Nucl. Instrum. Methods **186**, 453 (1981).
[17]B. K. Barnes, T. A. Belote, and J. R. Risser, Phys. Rev. **140**, 616 (1965).
[18]B. M. U. Scherzer, H. L. Bay, R. Behrisch, P. Børgesen, and J. Roth, Nucl. Instrum. Methods **157**, 75 (1978).
[19]J. S. Williams and W. Möller, Nucl. Instrum. Methods **157**, 213 (1978).
[20]Dr. H. Klingele, Adelgundenstrasse 8, 8000 München 22, Institut für Rasterelektronenmikroskopie (private communication).
[21]H. Stuessi, S. Veprek, and A. P. Webb, Radiat. Eff. Lett. **43**, 187 (1979).
[22]S. M. Myers, Nucl. Instrum. Methods **168**, 265 (1980).
[23]S. J. Kim, M. A. Nicolet, and R. S. Averback, Appl. Phys. A **41**, 171 (1986).
[24]A. S. Nowick and J. J. Burton, Diffusion in Solids (Academic, New York, 1975).
[25]T. Iwata, and H. Suzuki, *Proceedings of the Symposium on Radiation Damage in Solids and Reactor Materials* (IAEA, Vienna, 1963); T. Iwata, H. Maeta, and H. Matsuo, J. Phys. Soc. Jpn. **33**, 1060 (1972); T. Iwata, H. Maeta, and H. Matsuo, *ibid.* **36**, 123 (1974); T. Iwata, H. Maeta, and S. Okuda, *ibid.* **39**, 1558 (1975); T. Iwata, and T. Nihira, Jpn. J. Appl. Phys. **14**, 1099 (1975); T. Iwata, H. Maeta, and S. Okuda, Phys. Lett. **53A**, 295 (1975); T. Iwata, and T. Nihira, Jpn. J. Appl. Phys. **15**, 575 (1976).
[26]B. T. Kelly, W. H. Martin, A. M. Price, and J. T. Bland, Philos. Mag. **14**, 343 (1966).
[27]J. Roth, in *Physics of Plasma Wall Interactions, Controlled Fusion, Proceedings of the NATO Advanced Study Institute,* edited by D. E. Post and R. Behrisch, (Plenum, New York, 1986), p. 389.
[28]V. Phillips, E. Vietzke, and K. Flaskamp, Surf. Sci. **178**, 806 (1986).
[29]E. Hechtl and J. Bohdansky, J. Nucl. Mater. **141/143**, 139 (1986).
[30]E. Hechtl and Bohdansky, J. Nucl. Mater. **122/123**, 1431 (1984).
[31]Y. Gotoh, J. Nucl. Sci. and Technol. **18**, 641 (1981).